

Red Light-Responsive Upconverting Nanoparticles for Quantitative and Controlled Release of a Coumarin-Based Prodrug

Anaïs Brion, Juliane Chaud, Jérémie Léonard, Frédéric Bolze, Stefan Chassaing, Benoît Frisch, Béatrice Heurtault, Antoine Kichler,* and Alexandre Specht*

Photolytic reactions allow the optical control of the liberation of biological effectors by photolabile protecting groups. The development of versatile technologies enabling the use of deep-red or NIR light excitation still represents a challenging issue, in particular for light-induced drug release (e.g., light-induced prodrug activation). Here, light-sensitive biocompatible lipid nanocapsules able to liberate an antitumoral drug through photolysis are presented. It is demonstrated that original photon upconverting nanoparticles (LNC-UCs) chemically conjugated to a coumarin-based photocleavable linker can quantitatively and efficiently release a drug by upconversion luminescence-assisted photolysis using a deep-red excitation wavelength. In addition, it is also able to demonstrate that such nanoparticles are stable in the dark, without any drug leakage in the absence of light. These findings open new avenues to specifically liberate diverse drugs using deep-red or NIR excitations for future therapeutic applications in nanomedicine.

which is a particularly attractive release trigger.^[1–3] Recent years have witnessed technological improvements allowing photolytic reactions to become an interesting orthogonal trigger for the development of photochemical tools used today in many fields of biology.^[4–11] A chemical phototrigger refers to the use of a photolytic reaction to induce a dynamic process.^[12–18] In particular, photoremovable protecting groups (PPGs) have been used to mask the biological function of bioactive molecules.^[4–18] For biomedical applications, this method is extremely attractive since it allows for a light-controlled drug release to locally increase the concentration of an administered drug.^[19–22] The use of photocleavable linkers (PL), defined as bifunctional PPG derivatives that

can be linked to nanoparticles (NPs) and release a drug, can also solve both the usually poor solubility and the targeting ability of drugs directly coupled to PPGs.

However, to be useful for most in vivo applications, light-induced release from nanocarriers must be highly efficient and triggered by an optical wavelength that can innocuously penetrate deeply into tissues.^[1–3] Light penetration depth in skin and tissues is wavelength-dependent^[23] and most of the controlled drug-delivery systems are using photolytic reactions which respond to

1. Introduction


Nanoscale delivery systems which allow a noninvasive control of the release of bioactive molecules in living organisms are highly sought after.^[1,3] They are not only of interest in fundamental sciences, but they would also open up exciting perspectives for the treatment of diseases. Various strategies have been developed to trigger drug release by external stimuli, including light,

A. Brion, J. Chaud, B. Frisch, B. Heurtault, A. Kichler
3Bio Team
Laboratoire de Conception et Application de Molécules Bioactives
UMR 7199 Université de Strasbourg/CNRS
Faculté de Pharmacie
Illkirch F-67401 Cedex, France
E-mail: kichler@unistra.fr

J. Chaud, F. Bolze, A. Specht
Équipe de chimie et neurobiologie moléculaire
Laboratoire de Conception et Application de Molécules Bioactives
UMR 7199 Université de Strasbourg/CNRS
Faculté de Pharmacie
Illkirch F-67401 Cedex, France
E-mail: specht@unistra.fr

J. Léonard
Institut de Physique et Chimie des Matériaux de Strasbourg
Université de Strasbourg/CNRS
UMR 7504, Strasbourg F-67034, France

S. Chassaing
Institut de Chimie
Laboratoire de Synthèse
Réactivité Organiques & Catalyse
(LASYROC)
Institut de Chimie
UMR 7177 Université de Strasbourg/CNRS
Strasbourg F-67000, France

 The ORCID identification number(s) for the author(s) of this article can be found under <https://doi.org/10.1002/adhm.202201474>

© 2022 The Authors. Advanced Healthcare Materials published by Wiley-VCH GmbH. This is an open access article under the terms of the Creative Commons Attribution-NonCommercial License, which permits use, distribution and reproduction in any medium, provided the original work is properly cited and is not used for commercial purposes.

DOI: 10.1002/adhm.202201474

ultra-violet (UV) to blue light excitations. This is detrimental to biological or medical applications as those wavelengths are absorbed, scattered and are more toxic in living tissues than red or infra-red (IR) light. One attempt to solve this problem is based on tailoring the PPGs with extended π -conjugation and introducing heteroatoms and functional groups in the ring system to red-shift its absorption.^[24] While very efficient blue to green light-sensitive photoremovable groups have been reported using the coumarin scaffold,^[25–29] there is a dearth of PPGs with efficient responds to red or near infrared (NIR) light excitation.^[30]

In the last decade, the use of upconversion (UC), an anti-Stokes process converting red or NIR light into higher-energy photons, has emerged as a suitable option to trigger in vivo drug delivery upon photolysis from nanocarriers.^[31] For this purpose, inorganic lanthanide-based upconverting nanoparticles (L-UCNPs) have been widely studied.^[32–35]

However, they still suffer mostly from a high-power excitation requirement (10^1 – 10^4 W cm^{−2}) and inherently modest UC quantum yields owing to low absorption and emission cross-sections. Therefore, alternative and more biocompatible UC approaches have been developed, particularly using another type of UC systems based on triplet–triplet annihilation upconversion (TTA-UC) of organic chromophores.^[36–41]

In TTA-UC, photon energies absorbed by (at least) two sensitizer chromophores are transferred to emitter chromophores – also called “annihilators” – through collisions resulting in triplet–triplet energy transfer. Then, upon diffusion, two emitters in their triplet excited state may collide and undergo the TTA process, producing one singlet excited state emitting fluorescence at a shorter wavelength (Figure 1A,B).^[42–45] As a result, TTA-UC requires much lower excitation intensities than those needed by L-UCNPs (<0.1 W cm^{−2}) which could in turn open the door for life science applications. However, there are some major hurdles involved in applying TTA-UC for biological studies. Indeed, the mechanism of light UC by TTA is sensitive to molecular oxygen, which quenches the triplet states of the sensitizer and emitter, and further generates singlet oxygen (¹O₂) that can degrade the TTA-UC chromophores and cause toxicity to cells. Moreover, the TTA-UC chromophores are only soluble in organic solvents, limiting their use in cellular studies. To overcome these limitations, one strategy consists in the inclusion of the chromophores within nanoparticles.^[44] However, even then important challenges remain, as the stability of the NPs, the photolysis efficiency and the rates of drug leakage are important criteria to be optimized^[1–3,37–41] in order to develop such drug-delivery systems into useful tools for fundamental and applied sciences. Therefore, it is of crucial importance to develop platforms with improved robustness. Here, we designed TTA-UC nanoparticles based on the use of lipid nanocapsules (LNC) containing tetraphenyl-tetrabenzoporphyrin palladium (Pd-TPTBP) as triplet sensitizer and 2,5,8,11-tetra-*tert*-butylperylene (TBPe) as emitter. Our results show that LNC-UC nanoparticles present excellent photophysical properties with high UC efficiency in biological conditions and, notably, they surpass previously reported liposome-based Upconverting Nanoparticles (UC-NPs).^[45] In addition, we decorated this new class of TTA-UC nanoparticles for upconversion-assisted photolysis, using an efficient luminescence resonance energy transfer (LRET) process from the S₁ emitter state (produced by TTA-UC) to the photocleavable

group's acceptor anchored on the nanoparticle surface to achieve efficient drug delivery upon deep-red irradiation (Figure 1B). These light-activatable NPs were used to demonstrate that LNC based TTA-UC assisted drug-delivery systems can, after effective photorelease of the antitumoral drug melphalan, kill tumor cells in vitro and in vivo with a biocompatible deep-red-emitting LED.

2. Results and Discussion

2.1. Design of an Efficient and Biocompatible Nanopatform for Red to Blue Light UC Using TTA

To develop efficient deep-red to blue TTA-UC NPs, we used Pd-TPTBP as an organic sensitizer. As an emitter, we chose *tert*-butylated perylene instead of the well-studied perylene as the former was shown to be less prone to aromatic stacking and thus more soluble in the hydrophobic environment of the membranes.^[46] Previous studies have shown that this chromophore pair encapsulated in liposomes (Lps) enables UC with the use of antioxidants such as sodium sulfite or ascorbic acid to prevent oxygen quenching.^[44] We first wondered whether Lps are the most appropriate vehicles for TTA-UC due to the restricted diffusion possibilities of the hydrophobic chromophores inside the membrane bilayer. We therefore compared optimized liposomal formulations^[47] with a new type of UC nanoparticles based on lipid nanocapsules (LNC) which have a lipid core and an amphiphilic shell.^[48] Pd-TPTBP and TBPe, both highly hydrophobic, can be loaded quantitatively in the core of the LNC. Therefore, we formulated LNCs and Lps (see the Experimental Section) both loaded with the same concentration of UC chromophore pair (20×10^{-6} M of Pd-TPTBP and 200×10^{-6} M of TBPe, see Figure 1C for chromophores structures and Figure S1A in the Supporting Information for NP composition).

Successful loading of the sensitizer (Pd-TPTBP) and emitter (TBPe) into the NPs was confirmed by UV–Vis absorption spectroscopy of loaded LNCs and Lps (Figure S1E, Supporting Information), showing the characteristic bands of both Pd-TPTBP (at 630 nm) and TBPe (at 410 and 440 nm).

Moreover, compared to their respective spectra in solution, the absorption peaks of both the sensitizer and the emitter encapsulated in the nanocapsules did not shift significantly, indicating that neither sensitizer nor emitter aggregation occurred. We then characterized the obtained NPs using dynamic light scattering (DLS; see the Experimental Section and Figure S1B, Supporting Information). The two types of NPs loaded with UC molecules had roughly comparable diameters with 72 nm for the Lp and 56 nm for the LNC. Both NPs exhibit an almost neutral zeta surface potential (−3 and −9 mV for Lp-UC and LNC-UC respectively). Upon irradiation at 630 nm, the emission spectrum of both NPs solutions containing 10×10^{-3} M of the antioxidant ascorbic acid (Figure 1D) proved to be characteristic of the TBPe emission in the 430–560 nm range, thus demonstrating the UC process. In addition, we observed that the UC signal is more stable in LNC than Lp, since after 1 min of continuous irradiation at an intensity as high as ≈ 15 W cm^{−2}, the UC signal remains unchanged for the LNC while it decays by a factor of 4 for the liposomal formulation. Figure 1E displays a precise comparison of the UC efficiencies as a function of excitation light intensity, for both types of NPs with the same concentrations of UC chromophore

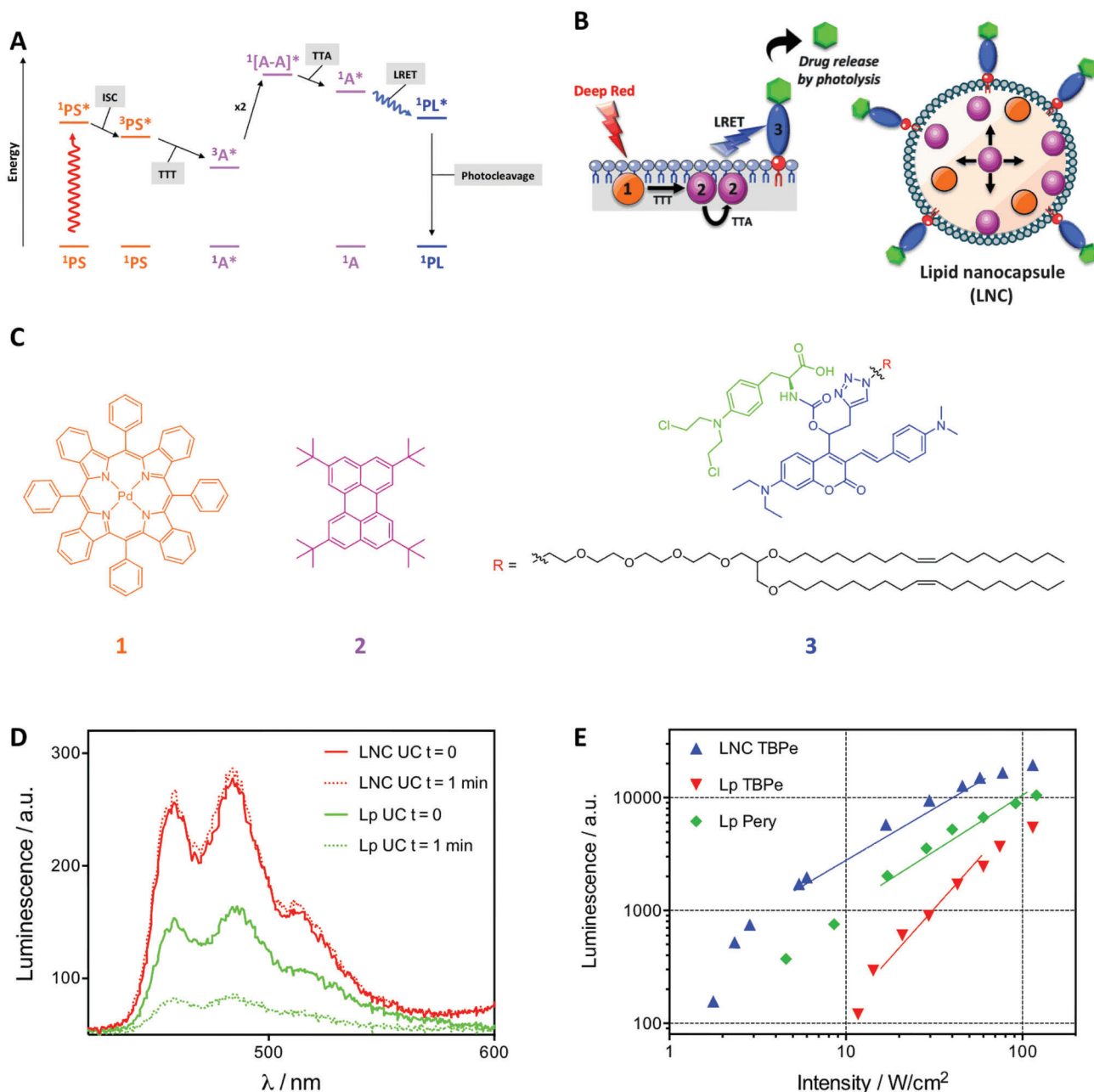


Figure 1. Formulation and luminescence properties of the upconverting nanoparticles. A) Jablonski diagram for the upconversion-assisted photolysis strategy: the photosensitizer (PS) absorbing red or NIR light ($^1PS^*$) goes into intersystem crossing (ISC) to generate triplet state ($^3PS^*$). Through collision, this energy is transferred to an emitter (A). This triplet-triplet transfer (TTT) leads to accumulation of emitters in their triplet state ($^3A^*$). When two $^3A^*$ collide, triplet-triplet annihilation (TTA) occurs and one emitter molecule reaches a singlet excited state ($^1A^*$) which may decay to ground state by luminescence emission of a higher energy photon, i.e., the so-called upconversion process. Here, rather than luminescence emission, the excitation energy of $^1A^*$ is transferred through luminescence resonance energy transfer (LRET) to the photocleavable linker (PL) leading to the photocleavage. B) Design of light-activable NP using TTA-UC assisted drug-delivery system: upconversion couple PS (1) and A (2) are integrated in the core of the LNC and the caged drug (3) is anchored at its surface allowing efficient deep-red light upconversion-assisted photolysis. C) Chemical structures of the photosensitizer PdTPBP (1), the emitter TBPe (2) and the photoactivatable prodrug DEACAS-DOG-Melph (3, composed of the photocleavable linker (PL), melphalan and a lipid anchor). D) Upconversion efficiency and stability depending on particle type: upconversion emission spectra of LNC with a diameter of 50 nm (red) and Lp (green) both loaded with the UC system (Pd-TPTBP 20×10^{-6} M and TBPe 200×10^{-6} M) in HEPES buffer supplemented with Na_2SO_3 50×10^{-3} M, recorded directly ($t = 0$, solid lines) and after 1 min ($t = 1$ min, dotted lines) irradiation of the sample, $\lambda_{ex} = 630$ nm ($15 W cm^{-2}$). E) Upconversion is more efficient in LNC-UC compared to others UC-NPs: emission signal (in arbitrary units "a.u.") integrated from $\lambda_{em} = 420$ to 560 nm as a function of excitation intensity with $\lambda_{ex} = 627$ nm for different UC-NPs: LNC and Lp, all loaded with the same amount of PS (Pd-TPTBP 10×10^{-6} M) and of A (Perylene or TBPe 100×10^{-6} M), in HEPES buffer supplemented with Na_2SO_3 50×10^{-3} M. The solid lines in this log-log graph are guides to the eye representing the linear (slope = 1; green and blue) or quadratic (slope = 2; red) regime of excitation. Lp and LNC are respectively the abbreviation for Liposome and Lipid NanoCapsules.

pairs, using either perylene or TBPe as the emitter. It reveals i) that the classical transition from the quadratic regime at lower excitation power to the linear regime at higher excitation power^[49] occurs at intensities depending critically on the NP type, and ii) the UC quantum yield of LNC-UC – defined in the linear regime – is 3 times higher than that previously reported for Lps,^[45] used as a reference here. Hence, at much lower intensities such as those used for in vivo drug release (see below), i.e., within the quadratic regime, the LNC-UC efficiency surpasses even more that of Lps. We propose that the increase of UC efficiency in LNCs may be explained by a more efficient diffusion process in the LNC core (Figure 1B, right) as compared to the Lps bilayer, thus increasing the rate of collisions between emitter triplet states.^[45]

Additionally, the higher hydrophobic volume and/or the presence of Lipoid S75 (which can act as an $^1\text{O}_2$ scavenger^[49]) in the LNCs surface might explain the stability of the signal over time. Taken together, our LNC-UCs show improved photophysical properties compared to the previously described UC-liposomes. Based on the UC quantum yield reported by Bonnet and co-workers,^[45] the UC quantum yield (Φ_{UC}) of our LNCs can be estimated at 0.054, leading to a useful brightness (defined as the product of the of the sensitizer's molar extinction coefficient [ϵ] at the excitation wavelength and the upconverted light generation quantum yield [ϕ_{em}]) for an UC-NP of $5\,700\text{ m}^{-1}\text{ cm}^{-1}$.

2.2. LNC: A Robust NP for light UC by TTA

We further investigated the TTA-UC properties of our nanoplat-form. First, the effect of the concentration of the TTA-UC chromophores inside the LNCs was evaluated (Figure S2C, Supporting Information). The results indicate that the LNC-UC formulated with Pd-TPTBP and TBPe at 60×10^{-6} and $600 \times 10^{-6}\text{ M}$, respectively, show the most interesting luminescence emission around 450 nm. However, for LNC with Pd-TPTBP and TBPe concentrations higher than 20×10^{-6} and $200 \times 10^{-6}\text{ M}$ respectively, a collisional quenching was observed. As expected, the system was sensitive to singlet oxygen (Figure S2A, Supporting Information) but a high and comparable emitted fluorescence intensity was observed after addition of sodium sulfite ($50 \times 10^{-3}\text{ M}$) or biologically relevant concentrations of ascorbic acid ($10 \times 10^{-3}\text{ M}$) (Figures S2A,D, Supporting Information). The presence of antioxidant is essential for efficient TTA-UC because oxygen strongly quenches the sensitizer triplet lifetime. Indeed, for NPs containing only Pd-TPTBP, the decay kinetics of the 800 nm phosphorescence reveals the sensitizer triplet state lifetime to be 200–300 μs in the presence of antioxidant (Na_2SO_3 or ascorbic acid) for both Lps and LNCs (Figure S2E, Supporting Information). For LNCs containing both Pd-TPTBP and TBPe in the presence of antioxidant, the 800 nm phosphorescence decays on the 16 μs time scale, which we assign to the triplet–triplet energy transfer (TTT) rate from Pd-TPTBP to TBPe (Figure S2E, right, Supporting Information). However, in the absence of antioxidant, the triplet state lifetime of Pd-TPTBP in LNCs is quenched on the 2.8 μs time scale, a rate faster than the TTT rate, thus impairing the second-order rise of the TBPe fluorescence signal (proportional to $[\text{TBPe}^*]^2$), hence the UC efficiency.^[50,51]

Of relevance for in vivo applications, we show in Figure S2A (Supporting Information) that the presence of 10% serum in the

culture medium only very weakly alters the UC signal, indicating that LNCs are stable in physiological conditions. It was also found that when stored at $+4\text{ }^\circ\text{C}$ for over a month or in mouse serum 24 h at $37\text{ }^\circ\text{C}$, the size of the LNCs did not change, which underlines the very good stability of the NPs (Figures S1C,D, Supporting Information). We next wondered whether using LNCs of smaller size could be advantageous. We therefore compared 50 nm diameter LNCs versus 20 nm ones formulated with roughly the same concentrations of sensitizer and emitter. The results showed that decreasing the size severely affects the UC efficiency indicating that the LNC internal volume can influence the UC efficiency (Figure S2B, Supporting Information).

Altogether, we were able to design a powerful system for red to blue light UC, producing intense and stable 430–470 nm light emission in biocompatible conditions. To go further, we then used the LNC-UCs to develop a new drug-delivery platform using coumarin-based PPGs.

2.3. Design and Synthesis of LNC-UCs Bearing a Blue Light-Sensitive Photocleavable Linker (PL)

To perform a TTA-UC assisted photolysis, a blue light-sensitive PL was synthesized. A coumarinyl scaffold, called DEACAS (for structure, see Figures 1C,2A), was selected because of its excellent uncaging efficiency upon blue light-excitation and its optimal absorption properties. This PPG was previously described to have an uncaging efficiency (defined as the product of the uncaging quantum yield [ϕ_u] and the molar extinction coefficient [ϵ]) of $8200\text{ m}^{-1}\text{ cm}^{-1}$ at 446 nm for the release of a carboxylic acid function.^[27] To be useful for the functionalization of TTA-UC NPs, the PPG was modified to introduce a lipid anchor which enables its incorporation into lipid-based delivery systems. Thus, a PL based on the DEACAS PPG was synthesized (see Figure 2A and Supporting Information for synthetic procedures). Since the LRET efficiency is dependent on the distance between the UC-induced TBPe S_1 states (trapped inside the particle) and the PL, a short triazole moiety between the PPG and the lipid anchor was selected to optimize the desired UC-assisted photolysis.

Starting from commercially available 7-*N,N*-(diethylamino)-4-methyl-2*H*-chromen-2-one **4**, the 7-*N,N*-(diethylamino)-2-oxo-2*H*-chromene-4-carbaldehyde **6** was synthesized with 78% yield in two steps.^[52] To obtain the DEACAS derivative with a propargyl function at the benzylic position, we decided to directly convert the stable aldehyde **6** to a coumarinyl derivative bearing a propargyl function at the benzylic position. The alkyne analogue **7** was obtained in 86% yield by the reaction of propargyl zincate with the aldehyde **6**. The compound **4** was converted to the brominated derivative **8** with 93% yield using *N*-bromosuccinimide. Notably, the reaction between **8** and freshly prepared *N,N*-dimethyl-4-[(*E*)-2-(4,4,5,5-tetramethyl-1,3,2-dioxaborolan-2-yl)ethenyl]aniline led to the formation of a more rigid coumarinyl PPG through domino reactions initiated by a 5-*exo*-dig cyclocarbopalladation.^[29] Therefore, we decided to graft first a diolelylglycerol (DOG- N_3) lipid anchor^[53] to the brominated derivative **8** via a CuAAC reaction which lead to the formation of **9** with 92% yield. Finally, the DEACAS-DOG **10** was obtained in 83% yield after a direct Suzuki reaction between **9** and

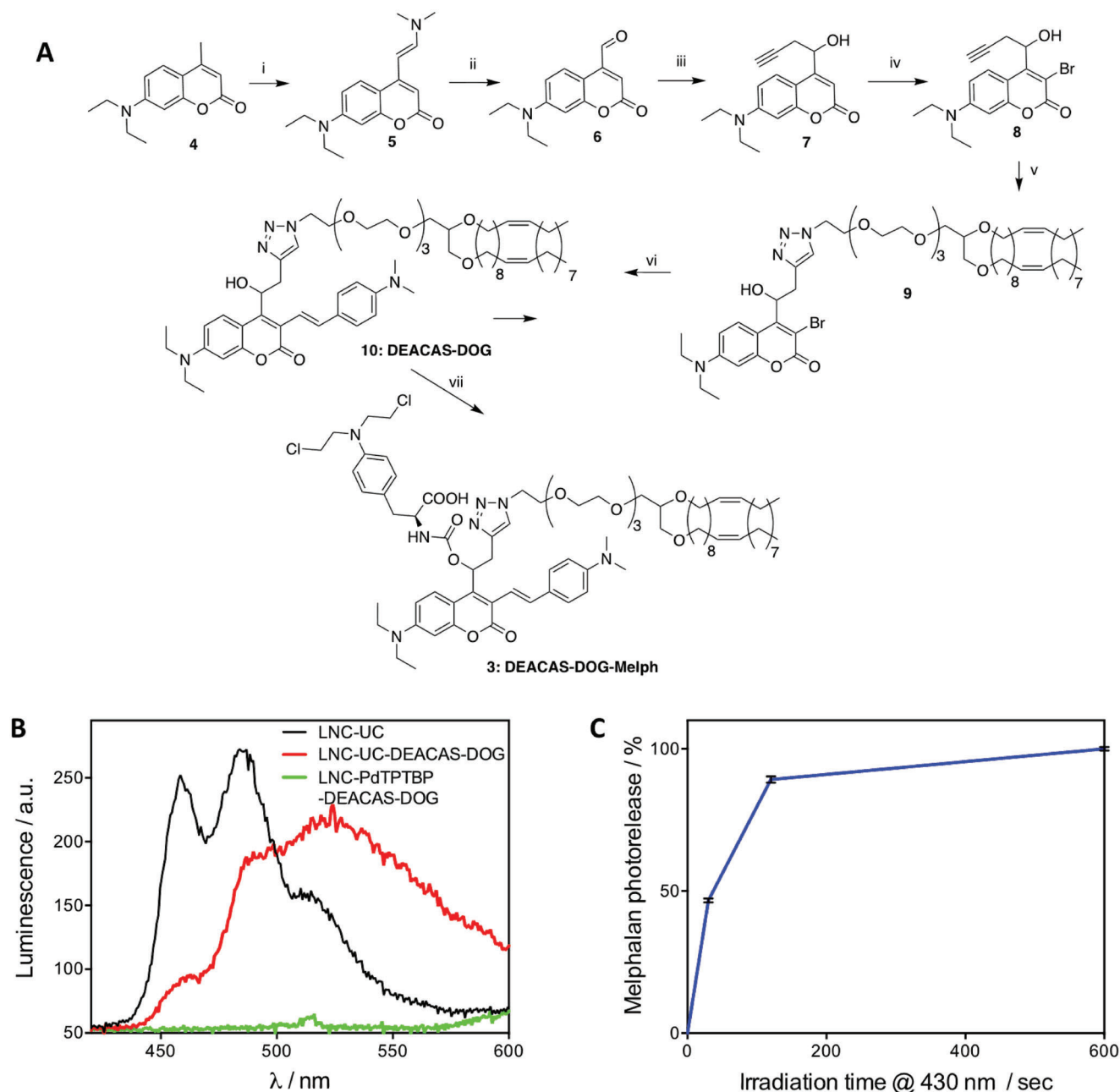


Figure 2. Robust and stable upconverting nanoplatform for UC and drug delivery: A) Synthesis of the fluorescent DEACAS-DOG analogue for the evaluation of the UC assisted LRET efficiency and the DEACAS-DOG-Melph prodrug: i) DMF-DMA, DMF, reflux, 16 h, quant., ii) NaIO_4 , THF/ H_2O , 0 °C to RT, 1 h, 78%, iii) Zinc propargyl bromide, THF, 0 °C to RT, 1 h 30, 86%, iv) NBS, ammonium acetate, anhydrous acetonitrile, RT, 30 min, 93%, v) (25Z)-1-azido-14-[(9Z)-octadec-9-en-1-yloxy]-3,6,9,12,16-pentaoxatetraatriacont-25-ene (DOG- N_3), ascorbic acid, distilled CH_2Cl_2 , tris(3-hydroxypropyl)triazolmethylamine, tetrakis(acetonitrile)copper (I) hexafluorophosphate, RT, 19 h, 92%, vi) *N,N*-dimethyl-4-[(*E*)-2-(4,4,5,5-tetramethyl-1,3,2-dioxaborolan-2-yl)ethenyl]aniline, K_2CO_3 , $\text{Pd}(\text{PPh}_3)_4$, $\text{H}_2\text{O}/\text{DME}$, in the microwave at 105 °C, 45 min, 83%, vii-a) *p*-nitrophenyl carbonate, DIPEA, DMF, RT, 8 h, vii-b) melphalan, DMAP, DIPEA, DMF, RT, 4 h 30, 82% over two steps. B) Emission spectra of LNCs upon 630 nm irradiation, loaded with either the UC system (LNC-UC, Pd-TPTBP/TBPe, black), the UC system and LRET acceptor (LNC-UC/DEACAS-DOG, red), or Pd-TPTBP and LRET acceptor (LNC Pd-TPTBP/DEACAS-DOG, green). $\lambda_{\text{ex}} = 630 \text{ nm}$, 15 W cm^{-2} . C) Blue light-mediated melphalan photorelease: kinetics of drug release from LNC-UC-Prodrug upon 430 nm irradiation (200 mW cm^{-2}) in HEPES buffer supplemented with ascorbic acid $10 \times 10^{-3} \text{ M}$, monitored by HPLC.

the freshly prepared *N,N*-dimethyl-4-[(*E*)-2-(4,4,5,5-tetramethyl-1,3,2-dioxaborolan-2-yl)ethenyl]aniline.^[54]

To determine the LRET efficiency, the DEACAS-DOG compound was used in the formulation of our LNC-UC leading to NPs with PLs anchored to its surface. We took advantage of the intrinsic fluorescent properties of the DEACAS-DOG 10 to evaluate the LRET efficiency from the UC system to the DEACAS chromophore in the LNC (Figures S3A,B for excitation and emission spectra of TBPe and DEACAS-DOG). For this purpose, LNCs containing Pd-TPTBP and DEACAS-DOG with TBPe (LNC-UC-DEACAS-DOG) or without TBPe (LNC-Pd-TPTBP-DEACAS-DOG), or with TBPe alone (LNC-UC) were formulated (see Experimental Section and Figures S3C,D, Supporting Information). Upon Pd-TPTBP excitation at 630 nm, the emission profile of LNC-UC-DEACAS-DOG is red-shifted as compared to LNC-UC (Figure 2B), while LNC-Pd-TPTBP-DEACAS-DOG exhibits no fluorescence at all. The LRET efficiency was quantified from absorbance and excitation spectra of the three types of LNCs, as explained in detail in the Methods (Figure S3C,D, Supporting Information). It was evaluated to be around 30% (Figure S3C, Supporting Information), a very significant yield that results from the specific design of this new nanoplatform.

2.4. Controlled Drug Release Upon Deep-Red Irradiation

Because of the excellent photophysical properties of our LNC-UC bearing a DEACAS PPG at its surface, we sought to construct a TTA-UC drug-delivery platform. Our strategy consisted in developing a system where, after uncaging, the prodrug (lipid anchor-coumarin-drug) converts into hydrophilic drug that is thus released from the NPs to kill tumor cells. Therefore, the antitumoral drug melphalan, which is FDA-approved for the treatment of multiple myeloma, was grafted to the DEACAS-DOG using the corresponding *p*-nitrophenol carbonate intermediate to obtain the DEACAS-DOG-Melph with 82% yield over two steps (see Figure 2A). The photolytic release of melphalan from precursor DEACAS-DOG-Melph was analyzed first by UV-Visible spectroscopy (Figure S4A, Supporting Information) after irradiation at 430 nm in MeOH/PBS buffer (pH 7.2; 1/1 v/v). The UV analysis showed a decrease in absorbance at 450 nm and an increase at 390 nm with an isobestic point at 416 nm, corresponding to the disappearance of the DEACAS chromophore and the formation of a DEAC subproduct.^[27] The DEACAS-DOG-Melph compound was used to prepare a LNC-UC bearing the melphalan drug at the surface using a carbamate linkage to the DEACAS PL.

To quantify the yield of melphalan release after uncaging, the as-prepared LNC-UC-Prodrug was irradiated first at 430 nm (using a commercial LED light source) and the melphalan release was quantified respectively by UV spectroscopy and HPLC analysis after membrane filtration to separate the NPs from small molecules (Figures S4B and S5, Supporting Information). Remarkably, an almost quantitative melphalan release was observed after 10 min of irradiation (Figure 2C). When we irradiated the as-prepared LNC-UCs with a 641 nm light-emitting diode (LED) (200 mW cm⁻²), 95% of the melphalan was released after 60 min. Importantly, similar results were obtained after long term storage at 4 °C and after 24 h at 37 °C in 50% mouse serum (Ta-

Table 1. Light-mediated melphalan release: quantification of released melphalan from LNC-UC-Prodrug upon 430 and 641 nm irradiation (both sources 200 mW cm⁻²) in HEPES buffer supplemented with Na₂SO₃ 50 × 10⁻³ M, monitored by UV-Visible absorption. Yield of photorelease was evaluated either on freshly formulated particles or after storage over 6 weeks at 4 °C or 24 h at 37 °C in 50% mouse serum.

Storage time	Irradiation	Drug photorelease
Freshly formulated	Non irradiated	ND
	@430 nm 10 min	100%
	@630 60 min	95%
6 weeks at 4 °C	Nonirradiated	ND
	@430 nm 10min	89%
24 h at 37 °C in 50% mouse serum	Nonirradiated	ND
	@430 nm 10min	86%

ble 1 and Figure S4D, Supporting Information). In addition, the HPLC analysis revealed that only melphalan was released without any trace of Pd-TPTBP or TBPe, showing the excellent stability of our LNC-UCs (Figure S5, Supporting Information). The quantum yields for melphalan release, as determined by competition with the DEACAS-*p*-MBA caged analogue developed by Zhu et al. (*p*-MBA = *p*-methoxybenzoic acid, 20% uncaging quantum yield^[27]) as a reference molecule, were 22% and 23% respectively for the DEACAS-DOG-Melph in MeOH/H₂O:1/1 (v/v) or for the LNC-UC formulated with 0.62% of DEACAS-DOG-Melph in a PBS buffer at pH 7.3 (Figure S4C, Supporting Information). This latter value agrees with the very good quantum yields observed with the DEACAS PPG.^[27]

Considering the outstanding photolytic yield performance reached by our system, we next asked whether our system can kill different tumor cell types in a light controlled manner.

2.5. In Vitro Tumor Cell Killing

First, the cellular delivery of LNCs containing or not TBPe (LNC-TBPe and LNC-BLK, respectively) was investigated using confocal microscopy and we found an efficient and rapid uptake of the nanoparticles by the MDA-MB-231 cells (Figure S6C, Supporting Information). Similar results were obtained using LNCs containing a fluorescein-labelled lipid (LNC-FITC) (Figure S6A, Supporting Information).

To better quantify the uptake, flow cytometry was done using the LNC-FITC and the results showed that 80% of the cells endocytosed NPs after 6 h of incubation (Figure S6B, Supporting Information). Then, the cellular toxicity of the NPs was evaluated on MDA-MB-231 cells after 48 h of incubation using a series of concentrations of empty LNCs (LNC-BLK) and LNC-UCs. The cell viability was similar for both types of treatments and importantly the results showed an absence of cytotoxicity of the LNCs at concentrations ≤0.2 mg mL⁻¹ (Figure 3A, Supporting Information).

Next, to demonstrate the feasibility of a light-controlled cell killing, we selected 3 different human tumoral cell lines, namely MDA-MB-231, THP1, and PC3. The cells were irradiated or not at low light intensity (628 nm, 5 mW cm⁻²; see set up in Figure S7A,C in the Supporting Information). The results show that for the three cell lines, the condition with 0.25 mg mL⁻¹ of

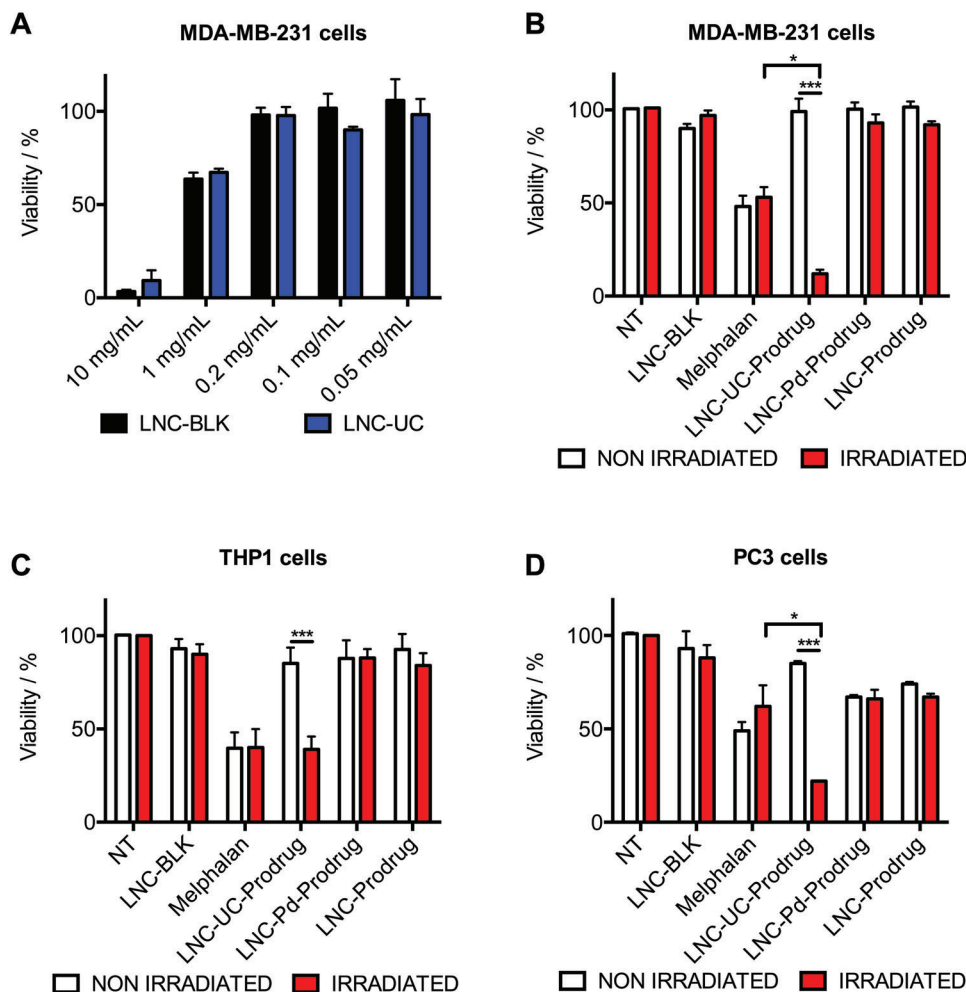


Figure 3. In vitro prodrug activation upon Deep-red irradiation. A) LNC-UC toxicity was determined by measuring cell viability of MDA-MB-231 cells after 48 h treatment with either empty LNCs (LNC-BLK, black) or LNC-UCs (blue) used at different amounts in the absence of irradiation. The cell viability was monitored using an MTS assay ($n = 3$). B–D) The viability of 3 tumor cell lines was determined after treatment +/- deep-red irradiation at low intensity ($\lambda_{\text{ex}} = 628 \text{ nm}$, 18 J cm^{-2} [5 mW cm^{-2} , 1 h]). See Figure S6 in the Supporting Information for set up. MDA-MB-231, THP1 and PC3 were treated with either melphalan (= free melphalan $1 \times 10^{-6} \text{ M}$), LNC-BLK (= empty LNC 0.25 mg mL^{-1}), LNC-UC-Prodrug (=LNC 0.25 mg mL^{-1} + Pd-TPTBP $0.05 \times 10^{-6} \text{ M}$ + TBPe $0.5 \times 10^{-6} \text{ M}$ + DEACAS-DOG-Melph $1 \times 10^{-6} \text{ M}$), LNC-Pd-prodrug (=LNC 0.25 mg mL^{-1} + Pd-TPTBP $0.05 \times 10^{-6} \text{ M}$ + TBPe $0.5 \times 10^{-6} \text{ M}$ + DEACAS-DOG-Melph $1 \times 10^{-6} \text{ M}$) or LNC-Prodrug (=LNC 0.25 mg mL^{-1} + DEACAS-DOG-Melph $1 \times 10^{-6} \text{ M}$), drug to light delay (DLI) 4 h. Cell viability was monitored at day 8 by cell counting after trypan blue staining ($n = 3$, *** $p < 0.01$, * $p < 0.05$).

LNC-UC-Prodrug (final concentration of Pd-TPTBP $0.05 \times 10^{-6} \text{ M}$, TBPe $0.5 \times 10^{-6} \text{ M}$, DEACAS-DOG-Melph $1 \times 10^{-6} \text{ M}$) a dramatic drop in the cell viability was observed after 628 nm light irradiation (Figure 3B–D).

Depending on the cell line, the viability was reduced by 88 to 61% while in the absence of irradiation the viability was similar to untreated cells. It is worth noting that the cytotoxicity of free melphalan (at the same concentration) was always lower than that of the irradiated prodrug LNCs owing probably to the enhanced cellular uptake of the prodrug in the LNCs. Indeed, low cellular entry of melphalan is a factor which limits its efficiency.^[52] For cells treated only with Pd-TPTBP $0.05 \times 10^{-6} \text{ M}$, DEACAS-DOG-Melph $1 \times 10^{-6} \text{ M}$ LNCs or with only DEACAS-DOG-Melph $1 \times 10^{-6} \text{ M}$ LNCs, no significant cytotoxic effects were observed with or without light irradiation demonstrating respectively negligible photodynamic therapeutic (PDT) effect of Pd-TPTBP in these

conditions, and that the cytotoxic effect is driven by a TTA-UC assisted photolysis. Also of importance, our results show that the lipid-based nanocapsules used at 0.25 mg mL^{-1} and containing Pd-TPTBP/TBPe are devoid of phototoxicity for all three tested cell lines.

2.6. Uncaging of the Prodrug Through Muscle Tissues

To evaluate the possibility to perform light-induced drug release through muscle tissue, we designed a deep-red irradiation set up through raw chicken breast (641 nm , 720 J cm^{-2} [200 mW cm^{-2} , 1 h]; see Figure 4A). As shown, the solution containing the LNC-UC-Prodrug is covered with meat of different thickness. After irradiation followed by gel filtration, we determined the melphalan photorelease by UV-visible spectroscopy. The results show an

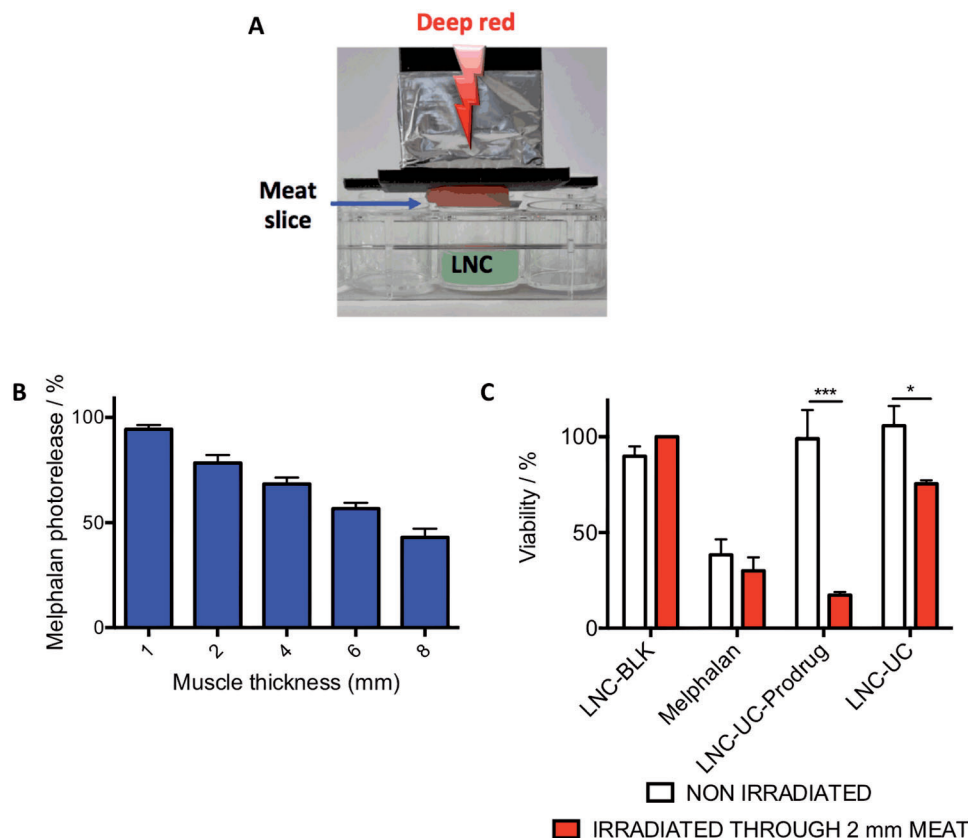


Figure 4. Quantification of melphalan photorelease through muscle slices. A) Setup used for deep-red irradiation through muscle slices ($\lambda_{\text{ex}} = 641 \text{ nm}$, 200 mW cm^{-2}). B) Melphalan release in solution upon deep-red irradiation through muscle: LNC-UC-Prodrug solution was irradiated ($\lambda_{\text{ex}} = 641 \text{ nm}$, 720 J cm^{-2} [200 mW cm^{-2} , 1 h]) through different chicken breast thickness. The yield of photoreleased melphalan was then monitored by UV-Visible absorption. C) Antitumoral activity of photoreleased melphalan on MDA-MB-231 cultured cells after irradiation through muscle slice: MDA-MB-231 cell viability after treatment with either Melphalan (=free melphalan $1 \times 10^{-6} \text{ M}$), LNC-BLK (=empty LNC 0.25 mg mL^{-1}), LNC-UC (=LNC 0.25 mg mL^{-1} + Pd-TPTBP $0.05 \times 10^{-6} \text{ M}$ + TBPe $0.5 \times 10^{-6} \text{ M}$) or LNC-UC-Prodrug (=LNC 0.25 mg mL^{-1} + Pd-TPTBP $0.05 \times 10^{-6} \text{ M}$ + TBPe $0.5 \times 10^{-6} \text{ M}$ + DEACAS-DOG-Melph $1 \times 10^{-6} \text{ M}$) +/− irradiation ($\lambda_{\text{ex}} = 641 \text{ nm}$, 720 J cm^{-2} [200 mW cm^{-2} , 1 h]) through 2 mm thick chicken breast. Cell viability was monitored by cell counting after trypan blue staining ($n = 3$) (* $p < 0.05$, *** $p < 0.01$).

almost quantitative photolysis through 1 mm of muscle tissue and a release that remains above 50% with 6 mm of muscle tissue (Figure 4B).

These very encouraging results led us to pursue cell killing assays. A 2 mm thick muscle slice was placed in front of the 641 nm LED system (641 nm , 720 J cm^{-2} [200 mW cm^{-2} , 1 h]) and the MDA-MB-231 cell viability after LNC treatment was evaluated (Figure 4C). Interestingly, for the cells treated with Pd-TPTBP $0.05 \times 10^{-6} \text{ M}$, TBPe $0.5 \times 10^{-6} \text{ M}$, DEACAS-DOG-Melph $1 \times 10^{-6} \text{ M}$ LNCs, the cell viability was dramatically decreased after 641 nm light irradiation with a higher effect than melphalan alone (17% of viability compared to 30%). To note, Pd-TPTBP $0.05 \times 10^{-6} \text{ M}$, TBPe $0.5 \times 10^{-6} \text{ M}$, LNCs showed a small phototoxicity (around 80% cell viability) that might be explained by a weak PDT effect when using higher light intensities (here 200 mW cm^{-2} as compared to 5 mW cm^{-2} used in experiments of Figures 3B–D). Together, we showed that the uncaging efficiency remains extremely high even through muscle slices and that our LNC-based system presents no leakage, since nonirradiated vehicles exhibited no toxicity.

These promising results allowed us to envisage in vivo applications and more specifically to evaluate the efficiency of the system in a mouse tumor model.

2.7. Evaluation of the TTA-UC Light-Controlled Uncaging of Melphalan on a Tumor Model

To show that our delivery system allows for an efficient release of melphalan after deep-red irradiation through the skin, we made the choice to inject directly the nanoparticles into the implanted tumors (while intravenous administration would add the extra step of accumulation of the NPs in the tumor). Briefly, the in vivo therapeutic efficacy of the LNCs was evaluated on MDA-MB-231 subcutaneous tumor-bearing nude mice (Figures 5A and Figure S7, Supporting Information). The mice were randomly divided in 5 groups, treated with either free melphalan ($3 \mu\text{g}$ per injection), LNC-UC (LNC 2.5 mg injection loaded with Pd-TPTBP 460 ng + TBPe $2.4 \mu\text{g}$) or LNC-UC-Prodrug (LNC 2.5 mg per injection loaded with DEACAS-DOG-Melph $3 \mu\text{g}$ + Pd-TPTBP

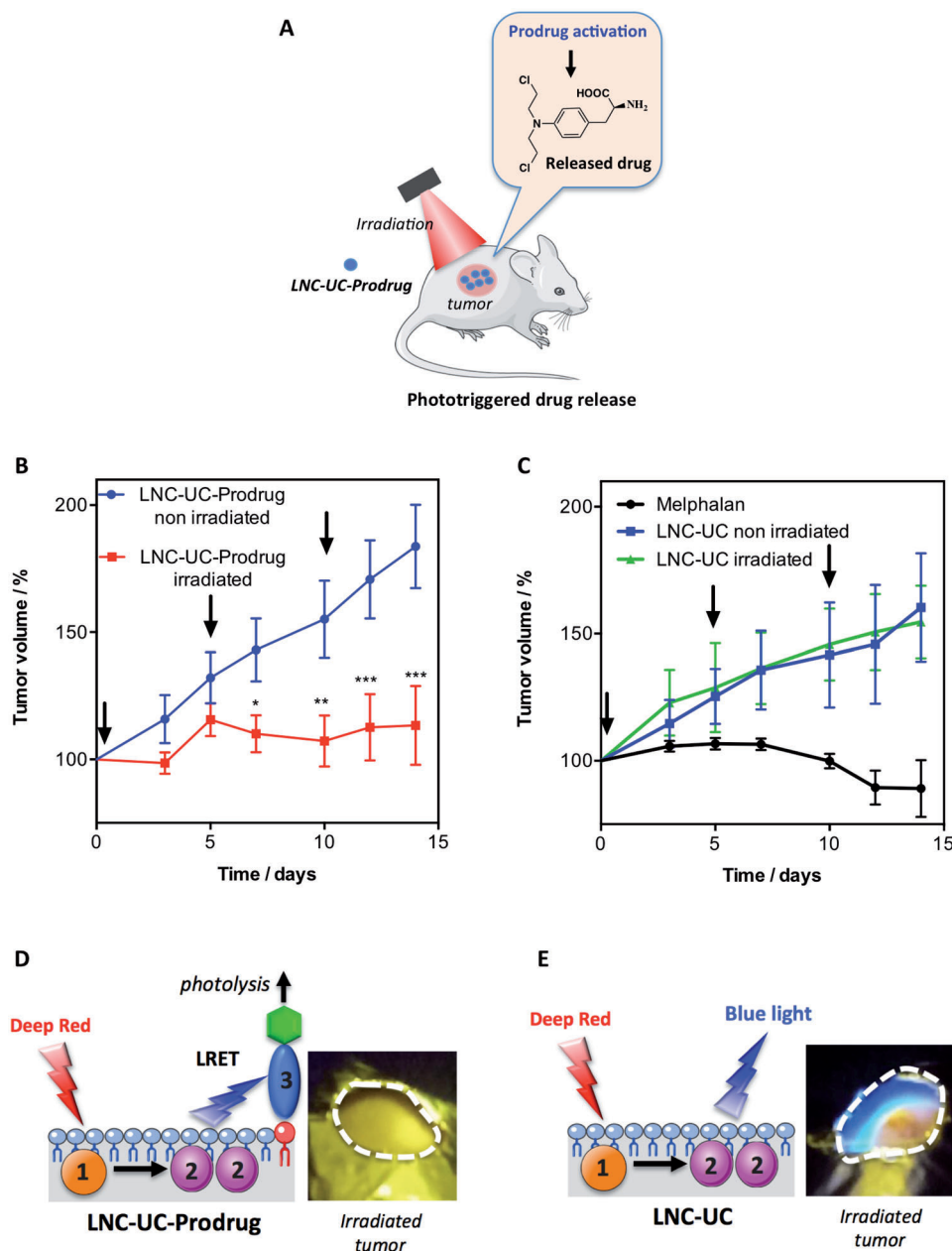


Figure 5. In vivo efficacy of the drug delivery system. A) Illustration of the LNC based TTA-UC assisted drug-delivery for effective photorelease of the antitumoral drug melphalan. B) Tumor growth inhibition by TTA-UC mediated drug release: relative tumor volume after LNC-UC Prodrug injection ($n = 7$ tumors per group, LNC 2.5 mg per injection loaded with DEACAS-DOG Melph 3 μg + Pd-TPTBP 460 ng + TBPe 2.4 μg), with and without irradiation (540 J cm^{-2} [200 mW cm^{-2} , $3 \times 15 \text{ min}$]); arrows represent the day of treatment. C) Tumor growth is not inhibited by LNC-UC treatment: relative tumor volume after LNC-UC ($n = 6$, LNC 2.5 mg per injection loaded with Pd-TPTBP 460 ng + TBPe 2.4 μg) or free Melphalan ($n = 4$, 3 μg per injection), with and without irradiation (540 J cm^{-2} [200 mW cm^{-2} , $3 \times 15 \text{ min}$]); arrows represent the day of treatment. D,E) Pictures and photos of tumors during LED deep-red irradiation after LNC injection: a blue light emission was visible after LNC-UC injection E) while it could not be observed after LNC-UC-Prodrug treatment D). * $p < 0.05$, ** $p < 0.02$, *** $p < 0.01$.

460 ng + TBPe 2.4 μg) with or without irradiation. Irradiation at 641 nm (540 J cm^{-2} [200 mW cm^{-2} , $3 \times 15 \text{ min}$]) was performed directly after the intratumoral injection of the LNCs (Figure S7B, Supporting Information, for set up). The treatment was repeated every 3 days. The treatment outcome of LNC-UC-Prodrug was assessed by monitoring the relative tumor volume in mice every 3 days.

The group treated with LNC-UC-Prodrug and 641 nm light irradiation showed good inhibition of tumor growth over 14 days (Figures 5B,D), while for the group treated with LNC-UC-Prodrug without light irradiation, the tumor volume quickly increased, indicating an important effect of the light-induced melphalan photorelease on tumor growth. In very good agreement with these observations is the fact that irradiated tumors injected

with LNC-UC produced a visible blue light (confirming a very efficient upconversion) while with LNC-UC-Prodrug injected tumors, no blue light was visible indicating that luminescence resonance energy transfer occurred efficiently (Figures 5D,E).

The group treated with only melphalan also showed an important inhibition of tumor growth over 14 days (Figure 5C) in agreement with the reported effect of melphalan on MDA-MB-231 cells.^[55,56]

Finally, for the groups treated with LNC-UC with or without light irradiation, the tumor volume quickly increased (Figures 5C,E), indicating no relevant PDT effect on tumor growth in vivo. A useful indicator for studying the toxicity and side effects of the LNCs is the fluctuation in body weight. As shown in Figure S8 (Supporting Information), the mice treated with our LNCs did not show weight loss, indicating that the delivery system was well supported.

3. Conclusion

In the present work, we have developed a simple method for the preparation of light upconverting LNCs able to efficiently convert red to blue light using Pd-TPTBP and TBPe for TTA-UC. In particular, we developed a new red light-sensitive platform based on lipidic nanocapsules (LNC) and our results show that a precise and covalent surface modification by blue light-sensitive coumarinyl PPG enables an efficient energy transfer from the LNC to the PPG (up to 30%). In addition, the DEACAS-DOG lipid can be easily coupled to an antitumoral drug such as melphalan using a stable carbamate link, allowing surface modification with a prodrug. Very importantly, the new platform allowed us to release more than 98% of the conjugated melphalan after a biocompatible irradiation using an LED. In addition, the LNCs showed an excellent stability in the dark and they were active in vitro even in the presence of serum. To the best of our knowledge, this is the first report of a stable light-sensitive nanoparticulate system able to quantitatively release a drug in the 630 nm spectral region. It is noteworthy that the uncaging efficiency at 630 nm of our photoactivatable NPs can be estimated around $560 \text{ m}^{-1} \text{ cm}^{-1}$, a value based on the absorption coefficient of Pd-TPTBP at 630 nm ($\epsilon_{630 \text{ nm}} = 105\,000 \text{ M}^{-1} \text{ cm}^{-1}$).^[57] the estimated UC quantum yield ($\Phi_{\text{UC}} = 0.054$), the 30% LRET efficiency energy transfer of the LNC-UCs to the DEACAS chromophore, and the uncaging quantum yield of DEACAS-DOG-Melph ($\Phi_{\text{u}} = 0.23$). We were also able to demonstrate that our LNCs can photorelease melphalan through meat slices with up to 8 mm thickness upon excitation with a 641 nm LED. In vitro studies on different cancer cell lines and in vivo studies on mice demonstrate that our LNC-based TTA UC-assisted drug-delivery system can effectively activate anticancer prodrug release in vitro and in vivo with a biocompatible deep-red LED light leading to a light-induced inhibition of tumor growths. It is to note that while our tumor model and injection route are not necessarily relevant in view of most clinical use, they allowed us to validate the fact that an efficient release of melphalan occurs after irradiation through the mouse skin. This paves the way for the evaluation of the delivery system in other models, in particular using intravenous or intraperitoneal injections.

In summary, we developed original light-activatable NPs able to release efficiently and quantitatively an anticancer drug us-

ing an excitation wavelength in the therapeutic window. We were also able to demonstrate that such LNCs are stable in the dark and able to quantitatively liberate a drug tethered to the surface of nanocapsules using a deep-red LED light source. The nanocapsules should allow versatile uses with modifiable properties like size, excitation/emission wavelengths and UC-assisted photolysis efficiencies, by doping with different TTA-UC sensitizer/emitter couples and by surface modification with red-shifted PPGs. The developed nanoplatfrom is not restricted to melphalan release but allows a great deal of flexibility to be used for a wide range of applications requiring programmed release of drugs or biological effectors by photoactivation. Therefore, our organic LNC-based TTA-UC assisted uncaging system offers a new platform for improving the performance of photoactivation systems for applications in biological studies, photoactivated chemotherapy, and targeted drug delivery.

4. Experimental Section

Synthetic Procedures: The synthetic procedures for the synthesis of the DEACAS-DOG **10** and the DEACAS-DOG-Melph **3** compounds are reported in the supporting information.

Lipid Nanocapsules Formulation: Pd-TPTBP, TBPe and DEACAS-DOG-Melph solubilized in a mix of chloroform/methanol (9/1 v/v) were first dried in the formulation vial. Thereafter, LNCs were formulated as described by Heurtault et al.,^[48] using a phase inversion method of an oil-water system. Briefly, the appropriate amount of each component, Labrafac, Solutol, Lipoid S75 and buffer, were added in a vial and heated under magnetic stirring up to 85 °C. After 3 cycles of heating up to 85 °C and cooling to 60 °C, ice cold buffer ($10 \times 10^{-3} \text{ M}$ HEPES, $150 \times 10^{-3} \text{ M}$ NaCl, $10 \times 10^{-3} \text{ M}$ ascorbic acid, pH 7.1) was added. The resulting LNC suspension was stirred for 5 min before further use. Control of UC molecules loading was assessed by UV-visible absorption after gel filtration of the LNC formulation.

Liposome Formulation: Multilamellar vesicles (MLV) were prepared by using a lipid film hydration technique as described previously by Jacobberger et al.^[58] Briefly, a chloroform/methanol solution (9/1 v/v) containing a mixture of lipids and light-sensitive molecules, were mixed in a round-bottom Pyrex tube, and was completely dried under high vacuum for 45 min. The resulting lipid film was then hydrated in $10 \times 10^{-3} \text{ M}$ HEPES, $150 \times 10^{-3} \text{ M}$ NaCl, pH 7.1 containing $10 \times 10^{-3} \text{ M}$ ascorbic acid at a final phospholipid concentration of $10 \times 10^{-3} \text{ M}$, leading to the formation of MLV. This suspension was then sonicated (1 s cycle every 3 s) during 1 h at room temperature under a continuous flow of argon, using a Vibra Cell 75041 ultrasonicator (750 W, 20 kHz, Fisher Bioblock Scientific) equipped with a 3 mm diameter tip probe (40% amplitude). The resulting small unilamellar vesicle (SUV) preparation was centrifuged at 13 000 g for 15 min to remove the titanium dust coming from sonication probes.

Particle Size Measurements: The average diameter of formulated nanoparticles was measured by dynamic light scattering using a Zetasizer Nano-ZS (MalvernPanalytical, UK) with the following specifications: viscosity: 1.014 cP; refractive index: 1.34; scattering angle: 90°; temperature: 25 °C. Particles were dispersed at 1/100 in $10 \times 10^{-3} \text{ M}$ HEPES buffer, $150 \times 10^{-3} \text{ M}$ NaCl, pH 7.1. Results are the average of three consecutive measurements. Data were analyzed using the multimodal number distribution software included with the instrument. Particle size was expressed in intensity. Samples are considered as monodisperse if the polydispersity index (PDI) is < 0.3.

Particle Zeta-Potential Measurements: Zeta-potential was determined at 25 °C using a Zetasizer Nano-ZS. Samples were dispersed at 1/50 in water and the zeta potential was calculated from the electrophoretic mobility based on the Smoluchowski approximation.

UC Luminescence Characterization: For high intensity excitation of the UC-NPs at 630 nm, a Tangerine laser system (Amplitude) delivering 300 fs

pulses centered at 1030 nm was used, at a repetition rate tunable from single pulse to 200 kHz. A home-made optical parametric amplifier pumped at 515 nm with the second harmonic of the Tangerine laser and seeded with a white light supercontinuum covering the visible to NIR range, is used to generate excitation pulses close to 630 nm as needed here, with up to 5 mW average power. This 630 nm beam was focused on a spot of diameter $\approx 60 \mu\text{m}$ inside a 0.5 mm thick cuvette containing the NP solutions, which enables reaching over 100 W cm^{-2} average excitation intensity (see Figure 1E).

The luminescence is collected and detected with a spectrograph equipped with a streak camera (Hamamatsu), which was used either in “focus” mode to monitor steady-state spectra (like in Figure 1D) or in “operate” mode to time-resolve the luminescence decay kinetics (like in Figure S2C in the Supporting Information) with a time-resolution depending on the observation time window (see details in Figure S2C in the Supporting Information).

UV-Vis Absorption and Fluorescence Measurements: Conventional UV-Vis spectroscopic measurements were carried out on a Safas Xenius XC apparatus, in a 3 mm spectroscopic cuvette. Fluorescence spectra recordings were conducted using the same set up when the 630 nm excitation was not needed. For fluorescence analysis, the samples were dispersed 1/100 in $10 \times 10^{-3} \text{ M}$ HEPES buffer, $150 \times 10^{-3} \text{ M}$ NaCl, pH 7.1 containing either $50 \times 10^{-3} \text{ M}$ Na_2SO_3 or $10 \times 10^{-3} \text{ M}$ ascorbic acid.

The TBP to DEACAS-DOG LRET efficiency was evaluated from the excitation spectra of two types of LNCs loaded with the UC chromophore pair (Pd-TPTBP $20 \times 10^{-6} \text{ M}$, TBP $200 \times 10^{-6} \text{ M}$) and with (a: LNC-UC-DEACAS-DOG) or without (c: LNC-UC) the LRET acceptor (DEACAS-DOG $280 \times 10^{-6} \text{ M}$), and a third type (b: LNC-Pd-TPTBP-DEACAS-DOG) missing the TTA emitter (Pd-TPTBP $20 \times 10^{-6} \text{ M}$, DEACAS-DOG $280 \times 10^{-6} \text{ M}$) as a negative control. With a detection wavelength fixed at 650 nm, one detects only the DEACAS-DOG fluorescence (TBP fluorescence occurs at shorter wavelengths). In Figure S4C (Supporting Information), A_A and A_D were defined as the absorbance at 414 nm (corrected from the scattering baseline) of the Acceptor DEACAS-DOG and of the Donor TBP, respectively, in the LNC. It was noted that Pd-TPTBP does absorb also around 440 nm (not shown) but not at 414 nm, which is the reason why 414 nm was chosen as the reference wavelength for the LRET efficiency evaluation. In Figure S4D (Supporting Information), F_A^A and F_A^D represent the Acceptor (DEACAS-DOG) fluorescence signals detected upon 414 nm excitation of the Acceptor, or of the Donor, respectively.

Since $(1 - 10^{-A_A})$ is proportional to the number of photons absorbed by the Acceptor, the ratio $F_A^A / (1 - 10^{-A_A})$ is proportional to (and may be used as a calibration for) the number of photons emitted by the Acceptor per photon directly absorbed at 414 nm by the Acceptor in this measurement. Similarly, the ratio $F_A^D / (1 - 10^{-A_D})$ is proportional (with the same calibrated, proportionality factor), to the number of photons emitted by the Acceptor per photon absorbed by the Donor TBP at 414 nm. Consequently, the LRET efficiency E_{LRET} is given by

$$E_{\text{LRET}} = \frac{F_A^D / (1 - 10^{-A_D})}{F_A^A / (1 - 10^{-A_A})} \quad (1)$$

Evaluating A_D , A_A , F_A^A , F_A^D at 414 nm as illustrated by the arrows in Figures S4C,D (Supporting Information), $E_{\text{LRET}} = 30\%$ was obtained (where the uncertainty was evaluated to $\pm 5\%$).

Determination of the Photochemical Quantum Yield: The quantum yield for the photoconversion was determined in MeOH/H₂O 9:1 (v:v) for the DEACAS-DOG-Melph and in HEPES $10 \times 10^{-3} \text{ M}$, NaCl $150 \times 10^{-3} \text{ M}$, pH 7.2 for LNCs formulated with the DEACAS-DOG-Melph at 25 °C by comparison with the DEACAS-*p*-methoxybenzoic acid described by Lin et al. ($\Phi = 0.2$) at the same concentration ($20 \times 10^{-6} \text{ M}$) as reference. 1 mL samples exposed to light, from a 1000 W Hg lamp from Hanovia (Radiant intensity in the 350–450 nm range: $10\,800 \text{ mW sr}^{-1}$) equipped with a water filter and focused on the entrance slit of a monochromator from Jobin-Yvon, France ($430 \pm 0.2 \text{ nm}$). The 430 nm monochromatic light was focused on the quartz cuvette. The reaction was monitored by UV spectroscopy on 1 mL for $20 \times 10^{-6} \text{ M}$ solutions of DEACAS caged pMBA^[27]

or DEACAS-DOG-Melph in MeOH/H₂O 9:1 (v:v) or formulated in LNCs. To determine the extent of the photolytic conversions, difference spectra (t_{irr}-t₀) were used. Full photolysis was confirmed by HPLC analysis for DEACAS caged pMBA.^[27] The absorbance decreases at 450 nm were plotted to follow the uncaging kinetics (k_{sample} for DEACAS-DOG-Melph or NC formulated DEACAS-DOG-Melph and k_{ech} for DEACAS caged pMBA), and values were normalized to full photolysis. The percentage of photolysis is plotted versus the irradiation time. A linear regression is then performed.

According to the following equation, the ratio of the rate constants is indeed directly proportional to the uncaging sensitivities of the new compound ($\epsilon_{\text{sample at 430 nm}} \times \Phi_{\text{sample}}$) and the reference compound ($\epsilon_{\text{ref at 430 nm}} \times \Phi_{\text{ref}}$)

$$\frac{k_{\text{sample}}}{k_{\text{ref}}} = \frac{\epsilon_{\text{sample}} * \Phi_{\text{sample}}}{\epsilon_{\text{ref}} * \Phi_{\text{ref}}} \quad (2)$$

Determination of the ϵ values at the excitation wavelength, measured in the solvent of the photolysis, then allowed the determination of the Φ_{sample} .

Quantification of Melphalan Release on LNCs: The full drug-delivery system that includes the DEACAS-DOG-Melph was formulated according to the previously explained method. Prior to irradiation, the samples were dispersed with the same buffer that was used in the formulation. Then the direct drug release from the LNC upon irradiation using 430 nm (using a LUMOS 43 LED source from Atlas Photonics Inc. based on UV-LED technology, with a typical output of 200 mW cm^{-2} and the wavelength of irradiation was set to 430 nm) or 641 nm light source (see below) was investigated by a membrane filtration of the sample using ultrafiltration unit (vivaspin 20) equipped with a 100 kDa cut-off semipermeable membrane (Sartorius Stedim Biotech, Aubagne, France). Vivaspin unit was then centrifuged at $5000 \times g$ for 20 min. Then, the eluate was analyzed either by HPLC or UV-Visible absorbance to evaluate the concentration of photoreleased melphalan. The same procedure was used for irradiation experiments through meat, adding a chicken breast slice above the irradiated sample. The row meat was cut and placed between two glass coverslips and the thickness was controlled using a vernier caliper (Helios Preisser, 821498).

LED Irradiation Sources for the In Vitro and In Vivo Experiments: A homemade irradiation apparatus was conceived for studies on 12 well plates. The 12 well irradiation apparatus consist of four raw connected in parallel of nine LED (red LED, 636 nm, 1100 mCd, Mouser 696-SSL-LX509E3SIT) connected in series. LEDs were soldered by group of three to allow irradiation of the 12 wells (Figure S7A, Supporting Information) and a 3D printed case was prepared to support 12 well plates. A variable laboratory power supply (BaseTech BT-305) was used to power the LED array with controlled voltage and intensity. The light power was measured for each well using a Thorlabs PM100D power meter. The spectrum of the LED used in this apparatus is shown in Figure S7C (Supporting Information) using the irradiation conditions ($\lambda_{\text{max}} = 628 \text{ nm}$, acquired using a Thunder Optics SMA-E spectrometer). The in vivo experiments were conducted using two 3 W 700 mA Avonect red LED 630 nm mounted with a heat sink on a flexible arm and drove by a dimmable 12 V constant current power source to fine tune the emitted light power. A 3D printed irradiation template allowing an irradiated zone of $1 \times 1 \text{ cm}^2$ with a distance LED-skin of 30 mm. The LED emission spectrum using the irradiation conditions is shown in Figure S7C (Supporting Information) ($\lambda_{\text{max}} = 641 \text{ nm}$, acquired using a Thunder Optics SMA-E spectrometer).

Cell Culture, In Vitro Irradiation, and Toxicity: MDA-MB-231 (human breast cancer cell line) and PC3 (human prostate adenocarcinoma) were obtained by ATCC. THP1 (human leukemic monocyte cell line) was obtained from Sigma-Aldrich. All cell lines were cultured in RPMI-1640 growth medium (Roswell Park Memorial Institute RPMI-1640 medium, Sigma Aldrich, UK), which originally includes L-Alanine, L-Glutamine and sodium bicarbonate. The medium was supplemented with 10% FBS (Fetal Bovine Serum), penicillin and streptomycin ($100/100 \text{ mg mL}^{-1}$). The cells were cultured at 37 °C in a cell incubator at 95% relative humidity with 5% CO₂ supply.

For the cell viability experiments using trypan blue counting, cells were seeded in 12-well plates at 1.6×10^4 cells per well in 1 mL of complete medium. 24 h after, cells were exposed to LNC treatment. Each well is treated with 0.25 mg mL^{-1} of LNCs, leading to a final concentration of $0.05 \times 10^{-6} \text{ M}$ of Pd-TPTBP, $0.5 \times 10^{-6} \text{ M}$ of TBPe and $1 \times 10^{-6} \text{ M}$ of DEACAS-DOG-Melph. After 4 hours drug to light delay (DLI), the cells were irradiated or not for 1 hour using a LED source at a power intensity of either 5 or 200 mW cm^{-2} . The same procedure was used for irradiation experiments through meat, adding a 2 mm chicken breast slice above the irradiated sample. The row meat was cut and placed between two glass coverslips and the thickness was controlled using a vernier caliper (Helios Preisser, 821498). After 5 days, cell number and viability were evaluated using trypan blue staining and cell counting using Countess 2 FL automated cell counter (ThermoFischer).

For the cell viability experiments using MTS assay, cells were seeded in 96-well plates at a density of 15×10^3 cells per well in 100 μL of RPMI-1640 medium. After 24 h, cells were treated while cells without treatment were used as control (viability = 100%). After 48 h, MTS cell viability assay was done by adding 20 μL of MTS (CellTiter 96 AQ_{ueous} One Solution Cell Proliferation Assay) to each well followed by incubation at 37°C for 30 min. Finally, the absorbance values of the full plate were measured at 490 nm using a microplate reader (Safas SP2000, Xenius 5801).

For the cellular uptake experiments, cells were seeded in glass coverslip in 12-well plates at 3×10^4 cells per well in 1 mL of complete medium. 24 h after, cells were exposed to LNCs (blank, or loaded with either TBPe $280 \times 10^{-6} \text{ M}$ or FITC $280 \times 10^{-6} \text{ M}$) treatment. FITC-PE (cat # 850332P, Polar Avantis Lipid) was added to LNC formulation where needed. Each well was treated with 0.25 mg of LNCs, leading to a final concentration of $0.7 \times 10^{-6} \text{ M}$ of TBPe or $0.7 \times 10^{-6} \text{ M}$ FITC. After 4 or 6 hours of incubation, the cells were washed twice in PBS, fixed using 4% *para*-formaldehyde solution during 10 min, washed again twice in PBS contained with cytoplasmic membrane dye CellBriteNIR680 (Biotium) for 10 min, washed again in PBS twice and the coverslips were mounted on glass slide. The samples were then observed on a Leica TCS SPE II confocal microscope.

For flow cytometry analysis, cells were seeded in glass coverslip in 12-well plates at 3×10^4 cells per well in 1 mL of complete medium. 24 hours after, cells were exposed to LNC-FITC. Each well was treated with 0.25 mg of LNCs, leading to a final concentration of $0.7 \times 10^{-6} \text{ M}$ FITC. After 0, 4 or 6 h of incubation, the cells were washed twice in PBS, trypsinized, washed twice again in PBS and the pellets were resuspended in PBS for analysis. Data were acquired on a BD FACSCanto (BD Biosciences) and analysis was performed with Flowjo software (version 10.2, Ashland, OR).

All in vitro experiments were conducted in technical and biological triplicates.

In Vivo Experiments: MDA-MB-231 cells (viability < 90% controlled with Count and viability, Muse, Millipore) were injected subcutaneously with 50% v/v of Matrigel HC (Corning, 354248) on both sides of Balb/c nude mice: 5×10^6 of cells/100 μL for each injection. When the average volume of tumors reached 100 mm^3 , the animals were divided in 5 groups, treated every 5 days (after isofluran anesthesia) with intratumoral injection (25 μL per tumor, Micro-fine+ syringe, BD) of either melphalan (3 μg per injection), LNC-UC (LNC 2.5 mg per injection loaded with Pd-TPTBP 460 ng + TBPe 2.4 μg) or LNC-UC-Prodrug (LNC 2.5 mg per injection loaded with DEACAS-DOG Melph 3 μg + Pd-TPTBP 460 ng + TBPe 2.4 μg). After injection of the formulations, animals were irradiated or not using a 200 mW cm^{-2} LED source using the following regime: $3 \times 15 \text{ min}$ irradiation with 1 min without irradiation in between to avoid excessive heating of the exposed area. The temperature was monitored and did not exceed 38°C on the irradiated skin. The tumor growth was monitored every 3 days using a vernier caliper (Helios Preisser, 821498). Study was conducted by the PCBIS platform (Illkirch, France) under local ethical committee agreement APAFIS no. #19214-2019021807554946.

Statistical Analysis: All data are presented as mean \pm SEM. All biochemical and in vitro experiments were conducted in triplicate and data are presented as mean \pm SEM. One-way (ANOVA) has been conducted to analyze the significance of the differences between the different conditions. A conclusion of a significant difference in results occurs when $p < 0.05$.

Supporting Information

Supporting Information is available from the Wiley Online Library or from the author.

Acknowledgements

This work was supported by the Université de Strasbourg, the CNRS, and by a Grant from the Agence Nationale de la Recherche (Contract No. ANR-18-CE09-0016). J.L. acknowledges the Interdisciplinary Thematic Institute QMat as part of the ITI 2021-2028 program of the University of Strasbourg, CNRS and Inserm via the IdEx Unistra (ANR 10-IDEX 0002), SFRI STRAT'US (ANR 20-SFRI 0012), and Labex NIE (ANR-11-LABX-0058-NIE) projects of the French Investments for the Future Program. B.F. and B.H. acknowledges the Interdisciplinary Institute HiFunMat, as part of the ITI 2021-2028 program of the University of Strasbourg, CNRS and Inserm via the IdEx Unistra (ANR-10-IDEX-0002) and SFRI-STRAT'US (ANR-20-SFRI-0012) under the framework of the French Investments for the Future Program. A.K. acknowledges the Interdisciplinary Institute InnoVec, as part of the ITI 2021-2028 program of the University of Strasbourg, CNRS and Inserm, via the IdEx Unistra (ANR-10-IDEX-0002) and SFRI-STRAT'US (ANR-20-SFRI-0012) under the framework of the French Investments for the Future Program. The authors thank Cendrine Seguin for assistance in the FACS experiments, the "Boucherie charcuterie KRESS SUGG" in Haguenau (France) for the preparation of the meat slices and Conor McCartin for proofreading of the manuscript.

Conflict of Interest

The authors declare no conflict of interest.

Author Contributions

A.B. and J.C. contributed equally to this work. J.C. and A.S. synthesized photoremovable linkers, J.C., S.C., and A.S. characterized the chemicals, J.C. A.B., J.L., F.B., and A.S. performed the photophysical and photochemical characterizations, A.B., B.H., F.B., B.F., and A.K. performed the in vitro and the in vivo experiments. All the authors analyzed the data, A.B., J.C., J.L., A.K., and A.S. wrote the paper. All authors discussed the results and commented on the manuscript, A.S., B.H., and A.K. designed the study and supervised the project.

Data Availability Statement

The data that support the findings of this study are available from the corresponding author upon reasonable request.

Keywords

photon upconversion, drug delivery, nanoparticles, photopharmacology, uncaging

Received: June 21, 2022
Revised: September 22, 2022
Published online: October 26, 2022

- [1] S. Mura, J. Nicolas, P. Couvreur, *Nat. Mater.* **2013**, 12, 991.
- [2] E.-K. Lim, T. Kim, S. Paik, S. Haam, Y.-M. Huh, K. Lee, *Chem. Rev.* **2015**, 115, 327.

- [3] X. Y. Wong, A. Sena-Torralba, R. Álvarez-Diduk, K. Muthoosamy, A. Merkoçi, *ACS Nano* **2020**, *14*, 2585.
- [4] S. Berlin, E. Y. Isacoff, *EMBO Rep.* **2017**, *18*, 677.
- [5] C. K. Kim, A. Adhikari, K. Deisseroth, *Nat. Rev. Neurosci.* **2017**, *18*, 222.
- [6] P. Paoletti, G. C. R. Ellis-Davies, A. Mouro, *Nat. Rev. Neurosci.* **2019**, *20*, 514.
- [7] D. Höglinger, A. Nadler, C. Schultz, *Biochim. Biophys. Acta* **2014**, *1841*, 1085.
- [8] G. Guglielmi, H. J. Falk, S. De Renzis, *Trends Cell Biol.* **2016**, *26*, 864.
- [9] A. Bardhan, A. Deiters, *Curr. Opin. Struct. Biol.* **2019**, *57*, 164.
- [10] B. Goegan, F. Terzi, F. Bolze, S. Cambridge, A. Specht, *ChemBioChem* **2018**, *19*, 1341.
- [11] A. Deiters, *Optochemical Biology in Methods in Enzymology*, Vol 624, Academic, San Diego, CA **2019**.
- [12] C. L. Fleming, M. Grøtli, J. Andréasson, *ChemPhotoChem* **2019**, *3*, 318.
- [13] M. M. Lerch, M. J. Hansen, G. M. van Dam, W. Szymanski, B. L. Feringa, *Angew. Chem., Int. Ed.* **2016**, *55*, 10978.
- [14] K. Hüll, J. Morstein, D. Trauner, in *Vivo Photopharmacol. Chem. Rev.* **2018**, *118*, 10710.
- [15] Y. Zheng, A. Farrukh, A. del Campo, *Langmuir* **2018**, *34*, 14459.
- [16] N. Ankenbruck, T. Courtney, Y. Naro, A. Deiters, *Angew. Chem., Int. Ed.* **2018**, *57*, 2768.
- [17] A. Gautier, C. Gauron, M. Volovitch, D. Bensimon, L. Jullien, S. Vriz, *Nat. Chem. Biol.* **2014**, *10*, 533.
- [18] C. Brieke, F. Rohrbach, A. Gottschalk, G. Mayer, A. Heckel, *Angew. Chem., Int. Ed.* **2012**, *51*, 8446.
- [19] J. S. Katz, J. A. Burdick, *Macromol. Biosci.* **2010**, *10*, 339.
- [20] N. Fomina, J. Sankaranarayanan, A. Almutairi, *Adv. Drug Delivery Rev.* **2012**, *64*, 1005.
- [21] G. Liu, W. Liu, C.-M. Dong, *Polym. Chem.* **2013**, *4*, 3431.
- [22] S. Bonnet, *Dalton Trans.* **2018**, *47*, 10330.
- [23] P. Juzenas, A. Juzeniene, O. Kaalhus, V. Iani, J. Moan, *Photochem. Photobiol. Sci.* **2002**, *1*, 745.
- [24] R. Weinstein, T. Slanina, D. Kand, P. Klán, *Chem. Rev.* **2020**, *120*, 13135.
- [25] L. Fournier, C. Gauron, L. Xu, I. Aujard, T. Le Saux, N. Gagey-Eilstein, S. Maurin, S. Dubruille, J. B. Baudin, D. Bensimon, M. Volovitch, S. Vriz, L. Jullien, *ACS Chem. Biol.* **2013**, *8*, 1528.
- [26] J. P. Olson, H.-B. Kwon, K. T. Takasaki, C. Q. Chiu, M. J. Higley, B. L. Sabatini, G. C. R. Ellis-Davies, *J. Am. Chem. Soc.* **2013**, *135*, 5954.
- [27] Q. Lin, L. Yang, Z. Wang, Y. Hua, D. Zhang, B. Bao, C. Bao, X. Gong, L. Zhu, *Angew. Chem., Int. Ed.* **2018**, *57*, 3722.
- [28] M. Klausen, V. Dubois, G. Clermont, C. Tonnelé, F. Castet, M. Blanchard-Desce, *Chem. Sci.* **2019**, *10*, 4209.
- [29] J. Chaud, C. Morville, F. Bolze, D. Garnier, S. Chassaing, G. Blond, A. Specht, *Org. Lett.* **2021**, *23*, 7580.
- [30] A. Y. Vorobev, A. E. Moskalensky, *Comput. Struct. Biotechnol. J* **2020**, *18*, 27.
- [31] S. Wu, H.-J. Butt, *Phys. Chem. Chem. Phys.* **2017**, *19*, 23585.
- [32] C.-J. Carling, F. Nourmohammadian, J.-C. Boyer, N. R. Branda, *Angew. Chem., Int. Ed.* **2010**, *49*, 3782.
- [33] J. Cao, S. Huang, Y. Chen, S. Li, X. Li, D. Deng, Z. Qian, L. Tang, Y. Gu, *Biomaterials* **2013**, *34*, 6272.
- [34] A. Bagheri, H. Arandiyán, C. Boyer, M. Lim, *Adv. Sci.* **2016**, *3*, 1500437.
- [35] S. Pearson, J. Feng, A. del Campo, *Adv. Funct. Mater.* **2021**, *31*, 2105989.
- [36] S. H. C. Askes, A. Bahreman, S. Bonnet, *Angew. Chem., Int. Ed.* **2014**, *53*, 1029.
- [37] L. Huang, Y. Zhao, H. Zhang, K. Huang, J. Yang, G. Han, *Angew. Chem., Int. Ed.* **2017**, *56*, 14400.
- [38] L. Huang, L. Zeng, Y. Chen, N. Yu, L. Wang, K. Huang, Y. Zhao, G. Han, *Nat. Commun.* **2021**, *12*, 122.
- [39] W. Lv, Y. Li, F. Li, X. Lan, Y. Zhang, L. Du, Q. Zhao, D. L. Phillips, W. Wang, *J. Am. Chem. Soc.* **2019**, *141*, 17482.
- [40] W. Lv, K. Long, Y. Yang, S. Chen, C. Zhan, W. Wang, *Adv. Healthcare Mater.* **2020**, *9*, 2001118.
- [41] K. Long, H. Han, W. Kang, W. Lv, L. Wang, Y. Wang, L. Ge, W. Wang, *J. Nanobiotechnol.* **2021**, *19*, 357.
- [42] D. K. K. Liu, L. R. Faulkner, *J. Am. Chem. Soc.* **1977**, *99*, 4594.
- [43] Y. Y. Cheng, B. Fückel, T. Khoury, R. G. C. R. Clady, N. J. Ekins-Daukes, M. J. Crossley, T. W. Schmidt, *J. Phys. Chem. A* **2011**, *115*, 1047.
- [44] S. H. C. Askes, S. Bonnet, *Nat. Rev. Chem.* **2018**, *2*, 437.
- [45] S. H. C. Askes, P. Brodie, G. Bruylants, S. Bonnet, *J. Phys. Chem. B* **2017**, *121*, 780.
- [46] S. H. C. Askes, W. Pomp, S. L. Hopkins, A. Kros, S. Wu, T. Schmidt, S. Bonnet, *Small* **2016**, *12*, 5579.
- [47] S. H. C. Askes, M. S. Meijer, T. Bouwens, I. Landman, S. Bonnet, *Molecules* **2016**, *21*, 1460.
- [48] B. Heurtault, P. Saulnier, B. Pech, J.-E. Proust, J.-P. Benoit, *Pharm. Res.* **2002**, *19*, 875.
- [49] Q. Liu, M. Xu, B. Tian, X. Zhang, F. Li, *ACS Appl. Mater. Interfaces* **2018**, *10*, 9883.
- [50] Y. Y. Cheng, T. Khoury, R. G. C. R. Clady, M. J. Y. Tayebjee, N. J. Ekins-Daukes, M. J. Crossley, T. W. Schmidt, *Phys. Chem. Chem. Phys.* **2012**, *12*, 66.
- [51] J. E. Auckett, Y. Y. Chen, T. Khoury, R. G. C. R. Clady, N. J. Ekins-Daukes, M. J. Crossley, T. Schmidt, *J. Phys.: Conf. Ser.* **2009**, *185*, 012002.
- [52] I. Elamri, M. Heumüller, L.-M. Herzig, E. Stirnal, J. Wachtveitl, E. M. Schuman, H. Schwalbe, *ChemBioChem* **2018**, *19*, 2458.
- [53] C. Salome, M. V. Spanedda, B. Hilbold, E. Berner, B. Heurtault, S. Fournel, B. Frisch, L. Bourel-Bonnet, *Chem. Phys. Lipids* **2015**, *188*, 27.
- [54] J. Kulhánek, F. Bureš, M. Ludwig, *Beilstein J. Org. Chem.* **2009**, *5*, 11.
- [55] G. J. Goldenberg, H. Y. Lam, A. Begleiter, *J. Biol. Chem.* **1979**, *254*, 1057.
- [56] G. Bernhardt, H. Reile, H. Birnböck, T. Spruss, H. Schönenberger, *J. Cancer Res. Clin. Oncol.* **1992**, *118*, 35.
- [57] C. Li, C. Koenigsmann, F. Deng, A. Hagstrom, C. A. Schmuttenmaer, J.-H. Kim, *ACS Photonics* **2016**, *3*, 784.
- [58] C. Jacobberger-Foissac, H. Saliba, M. Wantz, S. Seguin, V. Flacher, B. Frisch, B. Heurtault, S. Fournel, *Eur. J. Pharm. Biopharm.* **2020**, *152*, 348.